Competition between the nonadiabatic electronic state-mixing and the Herzberg-Teller vibronic effects in fluorescence process of tetraoxa[8] circulene

Valiev, R. R.

2020-01

Valiev , R R 2020 , ' Competition between the nonadiabatic electronic state-mixing and the Herzberg-Teller vibronic effects in fluorescence process of tetraoxa[8] circulene ' , Chemical Physics Letters , vol. 738 , 136914 . https://doi.org/10.1016/j.cplett.2019.136914

http://hdl.handle.net/10138/337219
https://doi.org/10.1016/j.cplett.2019.136914

Competition between the nonadiabatic electronic state-mixing and the Herzberg-Teller vibronic effects in fluorescence process of tetraoxa[8]circulene

R.R. Valiev[1,2]

[1]Tomsk State University, 36 Lenin Avenue, Tomsk, 634050, Russia

[2]University of Helsinki, Department of Chemistry, P.O. Box 55 (A.I. Virtanens plats 1), FIN-00014 University of Helsinki, Finland

Abstract

The effect of the nonadiabatic electronic state-mixing between the S_1 and S_2 states in tetraoxa[8]circulene is investigated computationally. The calculations show that the nonadiabatic electronic state-mixing effect on the fluorescence of tetraoxa[8]circulene is one million times weaker than the Herzberg-Teller vibronic effect. Analysis of the promotive modes of the $S_0 \rightarrow S_1$ and $S_1 \rightarrow S_0$ transitions shows that they are same for both absorption and emission. Also, the Duschinsky effect is found to be very weak for the $S_0 \rightarrow S_1$ and $S_1 \rightarrow S_0$ transitions. The Jahn–Teller symmetry breaking of the S_2 state leads to an energy splitting of ~1500 cm^{-1} between the two components of the S_2 state.

Keywords

Hetero[8]circulenes, tetraoxa[8]circulene, vibronic spectra, Jahn–Teller effect, Herzberg-Teller vibronic effect, nonadiabatic electronic state—mixing effect.

Introduction

Hetero[8]circulenes are a promising class of molecules for fabrication of organic light emitting diode (OLED) devices [1,2], organic field effect transistors (OFET) [3] and photodynamic therapy [4-7]. Tetraoxa[8]circulene (4B) is the first synthesized hetero[8]circulene; it was made as early as in 1968 [8]. 4B shown in Figure 1 has been found to have unique aromatic, spectroscopic and photophysical properties. The eight-membered carbon ring inside the molecule is called the hub and the perimeter of the molecule is the rim. Calculations of the magnetically induced current density showed that the hub sustains a paratropic ring current, whereas the ring current along the perimeter is of about the same size but in the opposite diatropic direction [9]. Thus, the hub is antiaromatic and the rim is aromatic according to the magnetic criteria. 4B can be globally nonaromatic, because it does not sustain any significant global ring current. Calculations of the magnetically induced ring current of the doubly charged 4B anion show that it is strongly aromatic, whereas the doubly charged cation is antiaromatic [10]. Current density calculations and calculations of spectroscopic properties have shown that there is a relation between aromaticity and low-lying excited states with strong

magnetic dipole transitions [11]. The first electronic excited singlet state (S_1) of neutral 4B absorbs in the blue region of the visible spectrum. It is a strong pure magnetic dipole transition. The $S_0 \rightarrow S_1$ transition of the antiaromatic 4B dication is also a strong magnetic dipole allowed transition that absorbs in the infrared region of the spectrum. The aromatic dianionic 4B does not have any low-lying strong magnetic dipole allowed transitions. The calculations showed that there is a correlation between the aromatic character and the spectroscopic properties of the 4B species, which has been found to hold also for other hetero[8]cirulenes and porphyrinoids [12-15].

The vibronically resolved absorption spectrum of 4B has also been simulated in the Franck-Condon and the Herzberg-Teller approximations including the Duschinsky effect [16]. The calculations showed that the vibrational mode of E_u symmetry at 1630 cm^{-1} and its combination with the A_{1g} mode at 1730 cm^{-1} contribute significantly to the vibronic progression of the $S_0 \rightarrow S_1$ transition. The A_{1g} mode at 1730 cm^{-1} has a large Huang-Rhys factor (y) of 0.85 and involves the hub atoms. Huang-Rhys factors are associated with the excitation probability of the vibrational modes during electronic excitation. Even though the mode at 1730 cm^{-1} alone is not active in the Herzberg-Teller approximation and consequently it does not appear in the vibronically resolved absorption spectrum of 4B, it strongly contributes to the hetero[8]circulene spectrum, where the $S_0 \rightarrow S_1$ transition is electric dipole allowed [2]. Since the vibrational mode at 1730 cm^{-1} of 4B has a large Huang-Rhys factor of 0.85, the rate constant for internal conversion (k_{IC}) between the S_1 and S_0 states of 10^7 s^{-1} is large [17, 18]. However, for other hetero[8]circulenes the A_{1g} mode has significantly smaller y values and therefore also smaller k_{IC} rate constants [17]. Thus, the spectroscopic and photopysical properties of 4B differ from those of many other hetero[8]circulenes due to the A_{1g} vibrational mode 1730 cm^{-1} with the large y value of 0.85. The specific hub structure of 4B is most likely responsible for the properties of the A_{1g} mode.

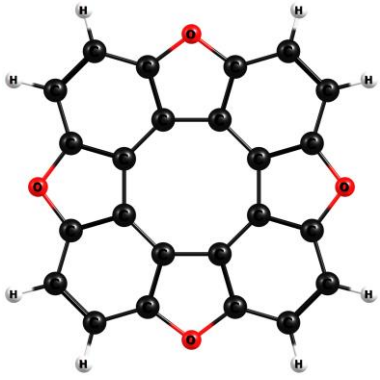

Figure 1. The molecular structure of 4B.

The $S_0 \rightarrow S_1$ transition of 4B is a pure magnetic dipole-allowed transition, which is forbidden in the electric dipole approximation. The $S_0 \rightarrow S_1$ transition appears at 415 nm in the electronic absorption spectrum of 4B according to previous calculations [16]. The fluorescence of 4B has a complicate character. It fluoresces at 508 nm with a quantum yield of 0.09. N. Karaush *et al.* explained the fluorescence based on of Herzberg-Teller theory [16]. The dependence of the electric transition dipole moment on the nuclear distance was found to be the main reason for the fluorescence at 508 nm [16]. However, the $S_0 \rightarrow S_2$ belongs to the E_u irreducible representation of the D_{4h} point group and it is strongly allowed in the electric dipole approximation [16]. The energy gap between the S_1 and S_2 states is about 4000 cm^{-1} according to time-dependent density functional theory (TDDFT) calculations using the B3LYP functional [16]. In such situations, the nonadiabatic electronic state-mixing of the S_1 and S_2 states can affect the fluorescence intensity and wavelength. For example, the nonadiabatic electronic state-mixing of the S_1 and S_2 states of pyrene has been found to be important [19]. The nonadiabatic electronic state-mixing effect is also important for polyacenes [17]. The goal of this work is to calculate and compare the fluorescence rate constants of 4B due to nonadiabatic electronic state-mixing and Herzberg-Teller vibronic effects.

Theory and computational details

The Herzberg-Teller vibronic effect

In a previous study, the vibronically resolved absorption spectrum of 4B was simulated in the Franck-Condon and Herzberg-Teller approximations including the Duschinsky effect [16]. Herzberg-Teller calculations including the Duschinsky effect are carried out and discussed in this work, since the influence of the Duschinsky effect was not emphasized in the previous study [16].

In the adiabatic approximation, the electric transition dipole moment can be written as

$$d_{01}^{HT} = << \varphi_0(r,R)\chi_0(R) | \hat{d}(r,R) | \varphi_1(r,R)\chi_1(R) >>_{r,R} =$$
$$= < \chi_0(R) | d_{01}(r,R) | \chi_1(R) >_R = d_{01}(r,R_0) \cdot < \chi_0(R) | \chi_1(R) >_R + \frac{\partial d_{01}(r,R)}{\partial R}|_{R=R_0} < \chi_0(R) | R | \chi_1(R) > \quad (1).$$

Here, $\hat{d}(r,R)$ is the dipole moment operator, R is the nuclear coordinate and r is the electronic coordinate, $\varphi_0(r,R)$ and $\varphi_1(r,R)$ are the electronic wavefunctions, and $\chi_0(R)$ and $\chi_1(R)$ are the nuclear wavefunctions corresponded to the ground S_0 and S_1 states.

When $d_{if}(r,R_0)$ is zero for $S_0 \rightarrow S_1$ or $S_1 \rightarrow S_0$ one has

$$d_{01}^{HT} = << \varphi_0(r,R)\chi_0(R) | \hat{d}(r,R) | \varphi_1(r,R)\chi_1(R) >>_{r,R} = \frac{\partial d_{01}(r,R)}{\partial R}|_{R=R_0} < \chi_0(R) | R | \chi_1(R) > \quad (2)$$

Here, $\frac{\partial d_{01}(r,R)}{\partial R}|_{R=R_0}$ is the derivative of the electronic transition dipole moment along the nuclear coordinate (R) at R_0. $<\chi_0(R)|R|\chi_1(R)>$ is the Herzberg-Teller factor. The values of both quantities have been calculated at the TDDFT level. The Duschinsky effect is considered in the harmonic approximation. The calculations have been performed using Gaussian 09 software [20]. The hessians of the initial and final states are needed for calculating $<\chi_0(R)|d_{01}(r,R)|\chi_1(R)>_R$ using Eq. (2). They have been obtained at the DFT and TDDFT level for the initial and final state, respectively. The Duschinsky transformation can be written in matrix form as [21]:

$$Q = JQ' + K \quad (3),$$

where Q and Q' are the coordinate vectors of the normal modes of initial and final electronic states, K describes the displacement of the oscillator equilibrium position and J is Duschinsky matrix. J approaches the unity matrix when the Duschinsky effect is small.

Here, d_{01}^{HT} including the Duschinsky effect is calculated for the $S_1 \rightarrow S_0$ transition using Eq. (2).

The nonadiabatic electronic state-mixing effect

The influence of nonadiabatic electronic state-mixing effect on $<<\varphi_0(r,R)\chi_0(R)|\hat{d}(r,R)|\varphi_1(r,R)\chi_1(R)>>_{r,R}$ for the transition between the S_1 and S_2 states can be estimated using:

$$\begin{aligned} d_{01}^{non} &= <<\varphi_0(r,R)\chi_0(R)|\hat{d}(r,R)|\varphi_1'(r,R)\chi_1(R)>>_{R,r} = \\ &= <<\varphi_0(r,R)\chi_0(R)|\hat{d}(r,R)|\varphi_1(r,R)\chi_1(R)>>_{r,R} + \\ &+ \sum_j c_{1j} <<\varphi_0(r,R)\chi_0(R)|\hat{d}(r,R)|\varphi_j(r,R)\chi_j(R)>>_{r,R} \end{aligned} \quad (3),$$

where $\varphi_1'(r,R) = \varphi_1(r,R) + \sum_j c_{1j}\varphi_j(r,R)$. c_{1j} can be obtained by using perturbation theory

$$c_{1j} = \frac{<<\varphi_1(r,R)\chi_1(R)|\Lambda(r,R)|\varphi_j(r,R)\chi_j(R)>>_{r,R}}{E_j - E_1} \quad (4).$$

where $\Lambda(r,R)$ is a nonadiabatic coupling operator [17] and E_j is energy of j-th singlet excited state. For 4B, the first term in Eq. (3) vanishes. Thus $c_{1i} <<\varphi_0(r,R)\chi_0(R)|\hat{d}(r,R)|\varphi_i(r,R)\chi_{in}(R)>>_{r,R}$ term makes the largest contribution to the nonadiabatic electronic state-mixing effect. The $<<\varphi_1(r,R)\chi_1(R)|\Lambda(r,R)|\varphi_j(r,R)\chi_j(R)>>_{r,R}$ strongly depends on the energy difference between the S_1 and S_j states [17]. TDDFT/B3LYP/def2-TZVP calculations show that the energy gap between S_1 and S_3 is ~6000

cm^{-1}, which is much larger than the energy gap of ~4000 cm^{-1} between the S_1 and S_2. The oscillator strength of $S_0 \rightarrow S_3$ is zero. The S_4 state is located ~10000 cm^{-1} above S_1. The oscillator strength of the $S_0 \rightarrow S_4$ transition is also zero. Therefore, only the second term in Eq. (3) with j=2 has to be considered when estimating the nonadiabatic electronic state-mixing effect, which is then obtained as

$$d_{01}^{non} = << \varphi_0(r,R)\chi_0(R) | \hat{d}(r,R) | \varphi_1'(r,R)\chi_1(R) >>_{R,r} = \\ = \frac{<< \varphi_0(r,R)\chi_1(R) | \Lambda(r,R) | \varphi_2(r,R)\chi_2(R) >>_{r,R}}{E_2 - E_1} < \chi_0(R) | d_{02}(r,R) | \chi_2(R) >_R = \quad (5).$$

The $< \varphi_0(r,R)\chi_1(R) | \Lambda(r,R) | \varphi_2(r,R)\chi_2(R) >>_{r,R}$ can be calculated in the adiabatic approximation [17]. S_2 state is degenerate since it belongs to the E_u irreducible representation. It is well known that Jahn–Teller effect leads to the spontaneous symmetry breaking [22]. The S_2 state splits into two non-degenerate states after the Jahn-Teller effect has been considered. The molecular structure of the non-degenerate S_2 state was obtained by performing molecular structure optimizations at the TDDFT/B3LYP/def2-TZVP level.

The transition moment d_{01}^{non} due to the nonadiabatic electronic state-mixing effect was calculated using Eq. (5). The oscillator strengths were obtained by using

$$f = \frac{2}{3} E_{10} d_{10}^2 \quad (6),$$

where d_{10} is d_{01}^{HT} and d_{01}^{non} fare used for the Herzberg-Teller and nonadiabatic electronic state-mixing channels, respectively.

Computational details

The optimized molecular structure and the hessian of the S_0, S_1 and S_2 states were calculated at the DFT and TDDFT levels using the B3LYP functional [23] and the def2-TZVP basis set [24]. The calculations were performed using the Gaussian software [25].

The d_{01}^{HT} transition moment was calculated at the TDDFT level of theory using the optimized molecular structure of the S_1 state employing the methodology described in Ref [20].

$< \varphi_1(r,R)\chi_1(R) | \Lambda(r,R) | \varphi_2(r,R)\chi_2(R) >>_{r,R}$ was calculated in the adiabatic and Franck-Condon approximation using the algorithm described in Ref. [17] without consideration for the Dushinsky effect and frequency change. According to the calculations the normal mode frequencies change only slightly (<5%), so they can be considered as equal for the S_1 and S_2 states. In addition, the Dushinsky effect does not influence the promotive modes of $S_2 \rightarrow S_1$ transition. Here

$$< \varphi_1(r,R)\chi_1(R) \mid \Lambda(r,R) \mid \varphi_2(r,R)\chi_2(R) >>_{r,R} =$$

$$= -\sum_{\nu} \sum_{q=x,y,z} M_{\nu}^{-1} < \varphi_1 \mid \frac{\partial}{\partial R_{q\nu}} \mid \varphi_2 > \left[\sum_{j=1}^{3N-6} B_{\nu qj} < 0_j \mid \frac{\partial}{\partial Q_j} \mid n_j > \prod_{\substack{k \neq j \\ k=1}}^{3N-6} < 0_k \mid n_k > \right] \quad (7),$$

where ν enumerates the nuclei, M_ν is mass of ν-th atom, $B_{\nu qj}$ are the matrix elements relating the displacements in Cartesian coordinates of the *ν-th* atom (ΔR_{q_ν}) and in the normal coordinate Q_j. The $\mid 0_k >$ and $\mid n_k >$ are harmonic oscillator wave functions of the initial and final states, n_k is the *n-th* excitation of *k-th* oscillator. In the terms $< 0_j \mid \frac{\partial}{\partial Q_j} \mid n_j >^2 = \frac{1}{2n_j!} \omega_j (n_j - y_j)^2 y_j^{n_j - 1} \cdot \exp(-y_j)$ and $< 0_k \mid n_k >^2 = \frac{\exp(-y_k) y_k^{n_k}}{n_k!}$ of Eq. (7), y_j is the Huang-Rhys factor and ω_j is the vibration frequency of *j*-th mode.

The complete active space self-consistent field (CASSCF) with the 10 electrons in 10 orbitals and state averaging over 4 lowest electronic states were used for calculating the nonadiabatic coupling matrix elements [26] at the second order perturbation theory (CASPT2) with the BAGEL software including static and dynamic electronic correlations [27]. The 6-31G(d,p) basis set was used in these calculations [28].

Result and discussion

The Herzberg-Teller vibronic effect

4B belongs to the D_{4h} point group. The first excited state (S_1) belongs to the A_{2g} irreducible representation. The promotive modes for both electronic transitions are listed in Table 1. The vibrational modes and the fluorescence spectrum of 4B are shown in Figure 2. All the peaks in the fluorescence spectrum are formed by the mode at 1693 cm^{-1} and its combination with the mode at 1704 cm^{-1} as in the case of absorption spectrum [16]. The elements of the Duschinsky J matrix of the promotive modes are given in Table 2. The data in Table 1 show that the E_u mode with an energy of 1653 cm^{-1} and its combination with the mode at 1718 cm^{-1} give the largest contributions to the transition moment of the $S_0 \rightarrow S_1$ transition. The same modes are also responsible for the fluorescence from S_1 to S_0. The calculations show that the influence of the Duschinsky effect on the $TDMI^2$ is small. The 91-th, 92-th and 93-th modes are though mixing implying that the B_{2g} mode does not appear as a promotive mode. The 94-th mode is localized in the hub and Duschinsky effect on that mode is negligible. The Duschinsky effect on the rate constants for internal conversion (k_{IC}) and intersystem crossing (k_{ISC}) is negligible, since it is small for the 94-th mode that is important for k_{IC} and k_{ISC} and the contributions to k_{IC} and k_{ISC} from the rest of the vibrational modes is very small [17,18]. The Duschinsky effect was not

accounted for in the previously calculated k_{IC} and k_{ISC} rate constants. However, the present calculations show that the Duschinsky effect does not significantly affect the previously reported k_{IC} and k_{ISC} rate constants of 4B [17, 18].

Table 1. The matrix elements of the Duschinsky matrix *J* for the promotive vibrational modes. $TDMI^2$ denotes the square of the transition dipole moment (in a.u.).

	With Dushinsky effect	$TDMI^2$ (a.u.)	Without Dushinsky effect	$TDMI^2$ (a.u.)
$S_0 \rightarrow S_1$	1653(E_u)	(0.42e-2)	1653(E_u)	(0.33e-2)
	1653(E_u)+1718 (A_{1G})	(0.33e-2)	1653(E_u)+1718(A_{1G})	(0.14e-2)
$S_1 \rightarrow S_0$	1693(E_u)	(0.36e-2)	1693(E_u)	(0.25e-2)
	1693(E_u)+1704(A_{1G})	(0.32e-2)	1693(E_u)+1704(A_{1G})	(0.13e-2)

Table 2. The Duschinsky *J* matrix. The prime indicates energies of the vibrational modes of the S_1 state.

Number of mode	91,1656 cm^{-1}, B_{2G}	92, 1693 cm^{-1}, E_U	93, 1693 cm^{-1}, E_U	94, 1704 cm^{-1}, A_{1G}
91', 1653 cm^{-1}, E_U	0.1e-3	-0.92	-0.28	0.2e-4
92', 1653 cm^{-1}, E_U	0.1e-3	0.28	0.93	-0.2e-4
93', 1670 cm^{-1}, B_{2G}	-0.85	0.2e-3	-0.9e-4	-0.9e-5
94', 1718 cm^{-1}, A_{1G}	-0.7e-5	0.1e-4	-0.2e-4	0.98

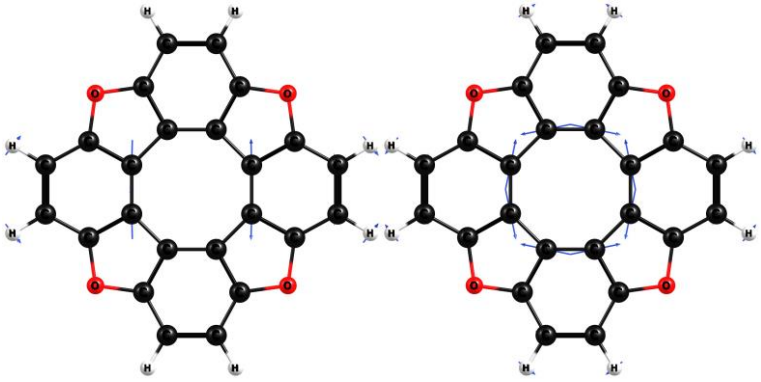

a) b)

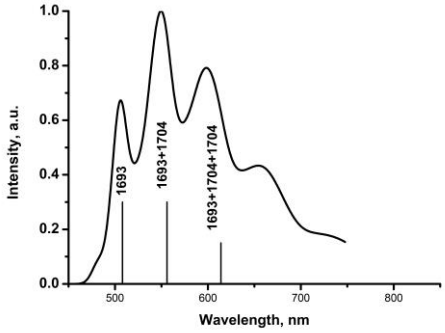

c)

Figure 2. The promotive modes for the $S_1 \rightarrow S_0$ and $S_0 \rightarrow S_1$ transitions of 4B. The E_u mode to the left has an energy of 1653 cm^{-1} and the energy of the A_{1G} mode shown to the right is 1718 cm^{-1}. Also, the fluorescence spectrum is shown below.

.

Almost the same d_{01}^{HT} value of 0.45 a.u. is obtained for the $S_1 \rightarrow S_0$ and $S_2 \rightarrow S_0$ transitions in the calculations. The oscillator strength due to the Herzberg-Teller effect (f_{01}^{HT}) is 0.01. On the other hand, f can also be estimated from the experimental absorption spectrum by using $f = 4.3 \cdot 10^{-9} \int \varepsilon(v) dv$, where ε is the extinction coefficient ($M^{-1}cm^{-1}$) and v is the energy in cm^{-1}. The estimated experimental oscillator strength is then 0.02, which was previously used for calculating the experimental radiative rate constant for 4B ($k_r = 9 \cdot 10^6$ s^{-1}) [17, 18] with the Strickler-Berg equation [29]:

$$k_r = \frac{1}{1.5} \cdot f \cdot E^2(S_1 \rightarrow S_0),$$

where f is the oscillator strength and $E(S_1 \rightarrow S_0)$ is the de-excitation energy from S_1 to S_0. The calculations suggest that Herzberg-Teller vibronic effect contributes at least 50% to the fluorescence quantum yield.

The nonadiabatic electronic state-mixing effect

The S_2 state belongs to the E_u irreducible representation and is degenerate in the ground-state structure. Optimizing the molecular structure of the S_2 state of 4B breaks the symmetry implying that S_2 is no longer degenerate. The optimized structure of the S_2 shown in Figure 3 belongs to the D_{2h} point group. The CASPT2 and TDDFT excitation energies are shown in Table 3. The schematic description of molecular orbitals (MOs) is given in Figure 4. The energy splitting between the symmetry-broken S_2' and S_2'' states is 1693 cm^{-1} and the energy difference between the S_1 and S_2' states is 4275 cm^{-1} according to the TDDFT calculations. S_2' and S_2'' denotes the two components of the former S_2 state, where the S_2'' state is assumed to be higher in energy. The CASPT2 calculation gives the energy gap between S_2' and S_2'' of 1371 cm^{-1}. Generally the CASPT2 and TDDFT energies agree well with each other. Also, the weight contribution and symmetry of electronic excited states are almost similar. The symmetry of S_2' and S_2'' are B_{3U} and B_{2U}. Thus, former $S_2(E_u)$ symmetry in D_{4h} splits into two nongenerate states with B_{3U} and B_{2U} irreducible representations in D_{2h} point group.

CASPT2 calculations of the non-adiabatic coupling elements give a value of 28 cm^{-1} for $< \varphi_1(r,R)\chi_1(R) \mid \Lambda(r,R) \mid \varphi_{2'}(r,R)\chi_{2'}(R) >>_{r,R}$, and $< \varphi_1(r,R)\chi_1(R) \mid \Lambda(r,R) \mid \varphi_{2''}(r,R)\chi_{2''}(R) >>_{r,R}$ is 10 cm^{-1}. The $c_{12'}$ and $c_{12''}$ coefficients then become 0.007 and 0.002, respectively. The $d_{2'0}$ and $d_{2''0}$ transition moments calculated at the TDDFT level are shows 0.36 a.u. and 0.32 a.u. yielding oscillator strengths of 0.24 and 0.21 for the $S_2' \rightarrow S_0$ and $S_2'' \rightarrow S_0$ transitions. The transition moment of the nonadiabatic channel d_{01}^{non} is

0.0032 yielding an oscillator strength of 10^{-6} for the nonadiabatic electronic state-mixing transition. The comparison of the oscillator strengths for the two channels shows that the nonadiabatic electronic state-mixing effect is negligible implying that the Herzberg-Teller vibronic effect is the main reason for the fluorescence of 4B.

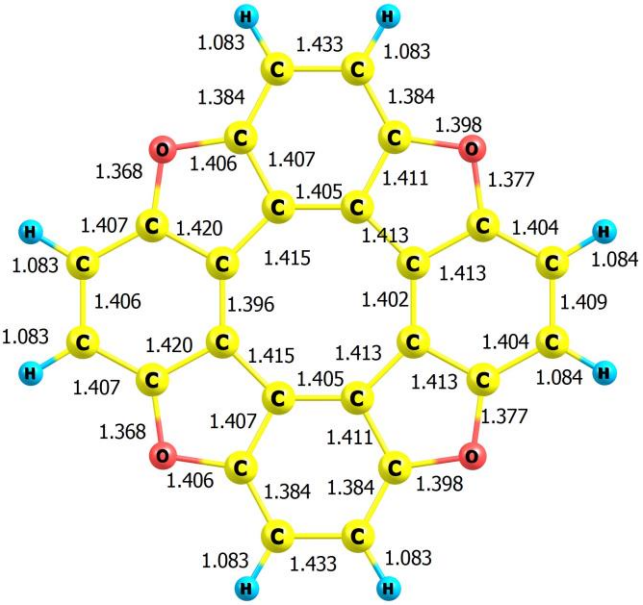

Figure. 3. The optimized molecular structure of the S_2' state.

Table 3. The TDDFT and CASPT2 excitation energies (eV), oscillator strengths in parenthesis, contributions of the most relevant transitions with their weights for 4B in D_{2h} point group geometry. Here H is HOMO and L is LUMO.

TDDFT			
State	Symmetry	the weights of the most relevant transitions	Energy(f)
S_1	B_{1G}	$H(b_{1u})\rightarrow L(a_u)$ 0.9;	2.71(0.0)
S_2'	B_{3U}	$H\text{-}1(b_{3g})\rightarrow L(a_u)$0.9;$H(b_{1u})\rightarrow L+1(b_{2g})$0.2	3.24(0.24)
S_2''	B_{2U}	$H\text{-}2(b_{2g})\rightarrow L(a_u)$0.96;$H(b_{1u})\rightarrow L+2(b_{3g})$0.2	3.45(0.22)
S_3	A_G	$H\text{-}3(a_u)\rightarrow L(a_u)$0.98	3.52(0.0)
S_4	A_G	$H\text{-}4(a_u)\rightarrow L(a_u)$0.95	4.21(0.0)
CASPT2			
State	Symmetry	the weights of the most relevant transitions	Energy(f)
S_1	B_{1G}	$H(b_{1u})\rightarrow L(a_u)$ -0.67	3.05(0.0)
S_2'	B_{3U}	$H\text{-}1(b_{3g})\rightarrow L(a_u)$-0.61	3.23(0.4)
S_2''	B_{2U}	$H\text{-}2(b_{2g})\rightarrow L(a_u)$0.61	3.40(0.3)

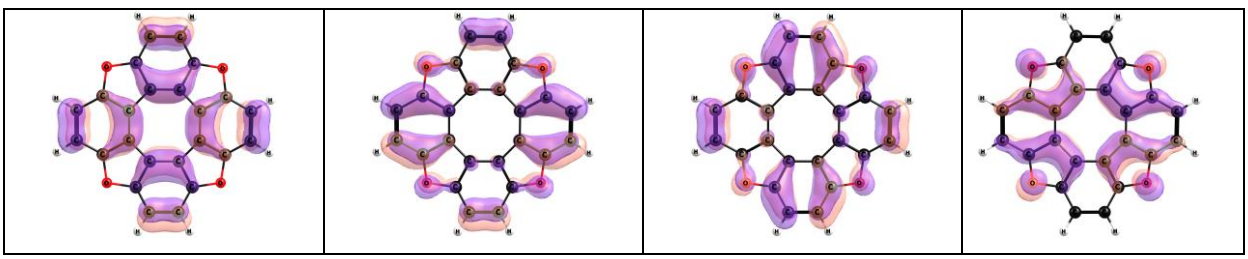

HOMO (b_{1u})	HOMO-1 (b_{3g})	HOMO-2 (b_{2g})	HOMO-3 (a_u)
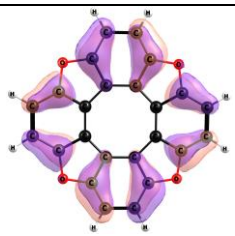	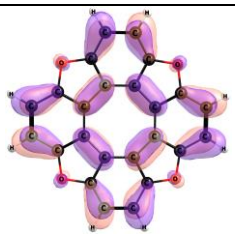	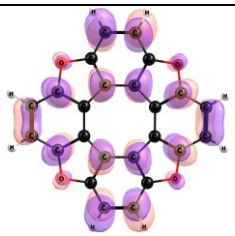	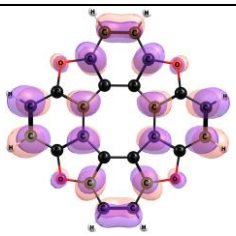
HOMO-4 (a_u)	LUMO (a_u)	LUMO+1 (b_{2g})	LUMO+2 (b_{3g})
DFT MOs			
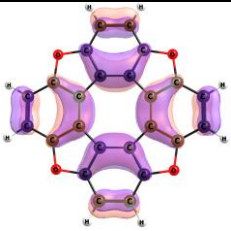	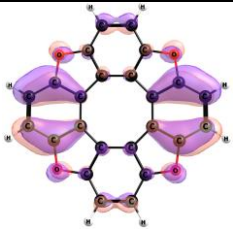	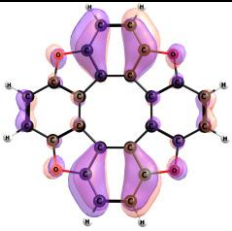	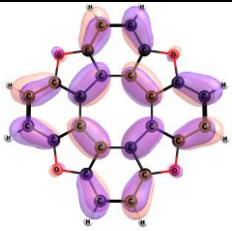
HOMO (b_{1u})	HOMO-1 (b_{3g})	HOMO-2 (b_{2g})	LUMO (a_u)
CASSCF MOs			

Figure 4. CASSCF and DFT molecular orbitals of 4B in S_2' state.

According to the calculation of the S_2' and S_2'' states, the excitations of 1703 cm^{-1} with y=0.35 and 656 cm^{-1} with y=0.3 give the main contribution to the Franck-Condon factor. The modes associated with C-H stretching give the main contribution to the vibrational integral $<0_j|\frac{\partial}{\partial Q_j}|n_j>$ because they have high frequency ~ 3000 cm^{-1} and small *y*~0. The shapes of modes of 656 cm^{-1} and 1703 cm^{-1} are given in Figure 5. The mode at 1703 cm^{-1} has smaller *y*=0.35 (compare with 0.85 for the D_{4h}) due to the changing symmetry of geometry from D_{4h} to D_{2h}. Both modes belong to the symmetry A_g according to the irreducible representation of D_{2h} group. In should be noted that the Dushinsky effects does not influence the promotive modes of $S_2' \rightarrow S_1$ and $S_2'' \rightarrow S_1$ transitions and C-H stretching modes. The Dushinsky matrix is almost unity for these vibrations.

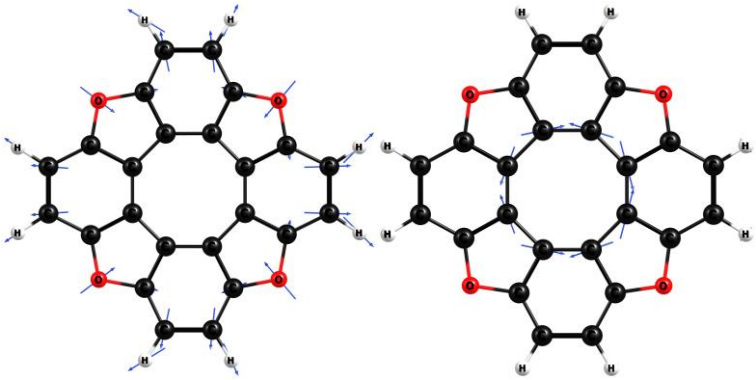

Figure 5. The promotive modes for the nonadiabatic electronic state-mixing effect of 4B in D_{2h} point group.

Since the oscillator strength due to the Herzberg-Teller effect is much larger than the oscillator strength due the the nonadiabatic electronic state mixing, one can conclude that the adiabatic approximation for S_1 and S_2 of 4B is accurate. Quantum chemical studies on the S_1 state of 4B can be carried out without considering the nonadiabatic electronic state-mixing effect. This is probably true also for other hetero[8]circulenes, since previously calculated spectroscopic and photophysical properties are in good agreement with experimental data without accounting for the nonadiabatic electronic state-mixing effect [2, 6, 7, 11, 16-18, 30-32].

Conclusion

The effect of the nonadiabatic electronic state-mixing between the S_1 and S_2 states of tetraoxa[8]circulene and the Herzberg-Teller vibronic effects have been investigated by performing DFT and TDDFT calculations. The Duschinsky effect was found to be very small for the $S_0 \rightarrow S_1$ absorption and $S_1 \rightarrow S_0$ emission involving the same vibrational modes. The nonadiabatic coupling matrix elements were calculated at the CASSCF level. The calculations show that the nonadiabatic electronic state-mixing effect is one million times less significant than the Herzberg-Teller vibronic effect. Optimization of the degenerate E_u state leads to symmetry breaking of the molecular structure from the D_{4h} point group of the ground state to the D_{2h} point group of the optimized S_2' state. The Jahn–Teller effect leads to the energy splitting of ~1500 cm^{-1} between the symmetry-broken S_2' and S_2'' states. The very small contribution from the nonadiabatic electronic state-mixing of the S_1 state explains why previously calculated photophysical and spectroscopic properties of 4B and other hetero[8]circulenes are in good agreement with experimental data, even though nonadiabatic state-mixing effects were neglected in the previous studies. The deviation of theoretical f=0.01 from the experimental estimate of 0.02 can be a reason of only 50% rather than 100% Herzberg-Teller contribution into

fluorescence process of 4B. This deviation is caused by the accuracy of quantum chemical calculation.

Acknowledgments

The research was carried out at the expense of the grant from Russian Science Foundation (project No. 17-73-20012) and the Academy of Finland (1325369).

References

[1] C. B. Nielsen, T. Brock-Nannestad, T. K. Reenberg, P. Hammershoj, J. B. Christensen, J. W. Stouwdam and M. Pittelkow, Organic light-emitting diodes from symmetrical and unsymmetrical π-extended tetraoxa[8]circulenes, Chem.: Eur. J. 16 (2010) 13030-13034. https://doi.org/10.1002/chem.201002261

[2] R. R. Valiev, R. M. Gadirov, K. M. Degtyarenko, D. V. Grigoryev, R. T. Nasubullin, G. V. Baryshnikov, B. F. Minaev, S. K. Pedersend, M. Pittelkow, The Blue Vibronically Resolved Electroluminescence of Azatrioxa [8] circulene, Chem. Phys. Let. 732 (2019) 136667. https://doi.org/10.1016/j.cplett.2019.136667

[3] T. Fujimoto, M. M. Matsushita, K. Awaga, Electrochemical field-effect transistors of octathio[8]circulene robust thin films with ionic liquids, Chem. Phys. Lett. 483 (2009) 81-83. https://doi.org/10.1016/j.cplett.2009.10.050

[4] Y. Serizawa , S. Akahori , S. Kato , H. Sakai , T. Hasobe , Y. Miyake and H. Shinokubo, Synthesis of Tetrasilatetrathia[8]circulenes by a Fourfold Intramolecular Dehydrogenative Silylation of C−H Bonds, Chem.: Eur. J. 23 (2017) 6948-6952. https://doi.org/10.1002/chem.201700729

[5] S. Akahori , H. Sakai , T. Hasobe , H. Shinokubo and Y. Miyake, Synthesis and Photodynamics of Tetragermatetrathia[8]circulene, Org. Lett. 20 (2018) 304-307. https://doi.org/10.1021/acs.orglett.7b03764

[6] G. V. Baryshnikov, R. R. Valiev, V. N. Cherepanov, N. N. Karaush-Karmazin, V. A. Minaev, B. F. Minaev and H. Ågren, Aromaticity and photophysics of tetrasila- and tetragerma-annelated tetrathienylenes as new representatives of the hetero[8]circulene family, Phys. Chem. Chem. Phys. 21 (2019) 9246-9254. https://doi.org/10.1039/C9CP01608B

[7] R. R. Valiev, G. V. Baryshnikov, V. N. Cherepanov, D. Sundholm, Ab Initio Study of Phosphorescence of Hetero[8]Circulenes, Rus. Phys. J. 62(3) (2019) 406-410. https://doi.org/10.1007/s11182-019-01727-7

[8] H. ErdtmanH, H.-E. Högberg, Cyclooligomerisation of quinones, Tetrahedron Lett. 11(38) (1970) 3389-3392. https://doi.org/10.1016/S0040-4039(01)98484-9

[9] G. V. Baryshnikov, R. R. Valiev, N. N. Karaush, B. F. Minaev, Aromaticity of the planar hetero[8]circulenes and of their doubly charged ions: NICS and GIMIC characterization, Phys. Chem. Chem. Phys. 16 (2014) 15367-15374. https://doi.org/10.1039/C4CP00860J

[10] G. Baryshnikov, R. R. Valiev, N. N. Karaush, D. Sundholm and B. Minaev, Aromaticity of the doubly charged [8]circulenes, Phys. Chem. Chem. Phys. 18 (2016) 8980-8992. https://doi.org/10.1039/C6CP00365F

[11] R. R. Valiev, G. V. Baryshnikov and D. Sundholm, Relations between the aromaticity and magnetic dipole transitions in the electronic spectra of hetero[8]circulenes, Phys. Chem. Chem. Phys. 20 (2018) 30239-30246 https://doi.org/10.1039/C8CP05694C

[12] R. R. Valiev, I. Benkyi, Y. Konyshev, H. Fliegl, D. Sundholm, Computational studies of the aromatic and photophysical properties of expanded porphyrins, J. Phys. Chem. A 122 (2018) 4756-4767. https://doi.org/acs.jpca.8b02311.

[13] R. R. Valiev, H. Fliegl, D. Sundholm, Closed-shell paramagnetic porphyrinoids, Chem. Commun. 53 (2017) 9866-9869. https://doi.org/10.1039/C7CC05232D.

[14] R. R. Valiev, H. Fliegl, D. Sundholm, Optical and magnetic properties of antiaromatic porphyrinoids, Phys. Chem. Chem. Phys. 19 (2017) 25979-25988. https://doi.org/10.1039/C7CP05460B.

[15] Isaac Benkyi, Heike Fliegl, Rashid R. Valiev and Dage Sundholm, New Insights on Aromatic Pathways of Carbachlorins and Carbaporphyrins Based on Calculations of Magnetically Induced Current Densities, Phys. Chem. Chem. Phys. 18 (2016) 11932-11941. https://doi.org/10.1039/C5CP06987D.

[16] N. N. Karaush, R. R. Valiev, G. V. Baryshnikov, B. F. Minaev, H. Ågren, DFT simulation of the heteroannelated octatetraenes vibronic spectra with the Franck–Condon and Herzberg–Teller approaches including Duschinsky effect, Chem. Phys. 459 (2015) 65-71. https://doi.org/10.1016/j.chemphys.2015.08.003

[17] R. R. Valiev, V. N. Cherepanov, G. V. Baryshnikov and D. Sundholm, First-principles method for calculating the rate constants of internal-conversion and intersystem-crossing transitions. Phys. Chem. Chem. Phys. 20(9) (2018) 6121-6133. https://doi.org/10.1039/C7CP08703A

[18] R. R. Valiev, V. N. Cherepanov, R. T. Nasibullin, D. Sundholm and T. Kurten, Calculating rate constants for intersystem crossing and internal conversion in the Franck-Condon and Herzberg-Teller approximations, Phys. Chem. Chem. Phys. (2019). https://doi.org/10.1039/C9CP03183A

[19] A. Ya. Freidzon, R. R. Valiev, A. A. Berezhnoy Ab Initio Simulation of Pyrene Spectra in Water Matrices, RSC Adv. 4 (2014) 42054-42065. https://doi.org/10.1039/c4ra05574h

[20] F. Santoro, A. Lami, R. Improta, J. Bloino and V. Barone, Effective method for the computation of optical spectra of large molecules at finite temperature including the Duschinsky and Herzberg–Teller effect: The Qx band of porphyrin as a case study, J. Chem. Phys. 128 (2008) 224311. https://doi.org/10.1063/1.2929846

[21] F. Duschinsky, The importance of the electron spectrum in multi atomic molecules. Concerning the Franck-Condon principle, Acta Physicochim. URSS. 7 (1937) 551.

[22] I. Bersuker, The Jahn-Teller Effect and Vibronic Interactions in Modern Chemistry, Springer US, New York, 1984. https://doi.org/10.1007/978-1-4613-2653-3

[23] C. Lee, W. Yang, R.G. Parr, Development of the Colle-Salvetti correlation-energy formula into a functional of the electron density, Phys. Rev. B. 37 (2) (1988) 785. https://doi.org/10.1103/PhysRevB.37.785

[24] F. Weigend and R. Ahlrichs, Balanced basis sets of split valence, triple zeta valence and quadruple zeta valence quality for H to Rn: Design and assessment of accuracy, Phys. Chem. Chem. Phys. 7 (2005) 3297-3305. https://doi.org/10.1039/B508541A

[25] M. J.Frisch, G. W.Trucks, H. B.Schlegel, G. E.Scuseria, M. A.Robb, J. R.Cheeseman, G.Scalmani, V.Barone, B.Mennucci, G. A.Petersson, H.Nakatsuji, M.Caricato, X.Li, H. P.Hratchian, A. F.Izmaylov, J.Bloino, G.Zheng, J. L.Sonnenberg, M.Hada, M.Ehara, K.Toyota, R.Fukuda, J.Hasegawa, M.Ishida, T.Nakajima, Y.Honda, O.Kitao, H.Nakai, T.Vreven, J. A.Montgomery Jr., J. E.Peralta, F.Ogliaro, M.Bearpark, J. J.Heyd, E.Brothers, K. N.Kudin, V. N.Staroverov, R.Kobayashi, J.Normand, K.Raghavachari, A.Rendell, J. C.Burant, S. S.Iyengar, J.Tomasi, M.Cossi, N.Rega, J. M.Millam, M.Klene, J. E.Knox, J. B.Cross, V.Bakken, C.Adamo, J.Jaramillo, R.Gomperts, R. E.Stratmann, O.Yazyev, A. J.Austin, R.Cammi, C.Pomelli, J. W.Ochterski, R. L.Martin, K.Morokuma, V. G.Zakrzewski, G. A.Voth, P.Salvador, J. J.Dannenberg, S.Dapprich, A. D.Daniels, O.Farkas, J. B.Foresman, J. V.Ortiz, J.Cioslowski and D. J.Fox, Gaussian 09, Revision A.1, Gaussian, Inc., Wallingford CT, 2009.

[26] W. H. Miller, Dynamics of Molecular Collisions, Plenum Press, New York, 1976. https://doi.org/10.1007/978-1-4757-0644-4

[27] BAGEL, Brilliantly Advanced General Electronic-structure Library. http://www.nubakery.org under the GNU General Public License.

[28] V.A. Rassolov, J.A. Pople, M.A. Ratner, T.L. Windus, 6-31G* basis set for atoms K through Zn, J. Chem. Phys. 109 (4) (1998) 1223-1229. https://doi.org/10.1063/1.476673

[29] S. J. Strickler and R. A. Berg, Relationship between Absorption Intensity and Fluorescence Lifetime of Molecules, Chem. Phys. Lett. 37 (1964) 814−822. https://doi.org/10.1063/1.1733166

[30] G. V. Baryshnikov, R. R. Valiev, N. N. Karaush, V. A. Minaeva, A. N. Sinelnikov, S. K. Pedersen, M. Pittelkow, B. F. Minaev, H. Agren, Benzoannelated aza-, oxa- and azaoxa[8]circulenes as promising blue organic emitters, Phys. Chem. Chem. Phys. 18 (2016) 28040-28051. https://doi.org/10.1039/C6CP03060B

[31] G. V. Baryshnikov, R. R. Valiev, B. F. Minaev, H. Agren, Substituent-sensitive fluorescence of sequentially N-alkylated tetrabenzotetraaza[8]circulenes, New J. Chem. 41 (2017) 7621-7625. https://doi.org/10.1039/C7NJ01599B

[32] G. V. Baryshnikov, R. R. Valiev, B. F. Minaev, H. Agren. A computational study of aromaticity and photophysical properties of unsymmetrical azatrioxa[8]circulenes. New J. Chem. 41 (2017) 2717-2723. https://doi.org/10.1039/C6NJ03925A